

Composition of the Interstellar Medium

by

P. Gnaciński and M. Krogulec

Institute of Theoretical Physics and Astrophysics,
University of Gdańsk, ul. Wita Stwosza 57, 80-952 Gdańsk, Poland
e-mail: pg@iftia.univ.gda.pl, fizmkr@univ.gda.pl

Received ...

ABSTRACT

We present an analysis of the Fe II, Ge II, Mg I, Mg II, S I, S II, Si II and Zn II interstellar lines for 63 stars. The column density of Mg II, S II, Si II and Zn II is well correlated with the distance. However, the column density – distance relation should be used with care for the estimation of the distance to OB stars. For stars with large $f(H_2)$ this relation can lead to a large overestimation of the distance. Hydrogen – normalised column densities of Mg II, Si II and Ge II (our largest samples of data) drop with the interstellar reddening $E(B-V)$ as expected for elements that are incorporated into dust grains. The Ge II abundance (G_{II}/H) is lower in dense molecular clouds. The abundances of all analysed elements are generally lower than their Solar System values.

Key words: *ISM: abundances — ultraviolet: ISM*

1 Introduction

McKee & Ostriker (1977) in their model have divided the interstellar medium (ISM) into three components: a low density hot ionised medium (HIM, $n \sim 10^{-2.5} \text{ cm}^{-3}$, $T \sim 10^{5.7} \text{ K}$), a dense cold neutral medium (CNM, $n \sim 10^{1.6} \text{ cm}^{-3}$, $T \sim 10^{1.9} \text{ K}$) and a photoionized cloud corona ($T \sim 8000 \text{ K}$). The cloud corona itself was divided into two subregions: warm ionized medium (WIM, fractional ionization $x_{\text{WIM}} \sim 0.7$), and a warm neutral medium (WNM, $x_{\text{WNM}} \sim 0.1$). The filling factor of the cloud corona was estimated to be $f \sim 0.2$, while the filling factor for the HIM was estimated to be $f \sim 0.7 \div 0.8$. The cold, dense clouds fill only $f \sim 0.02 \div 0.04$ of the interstellar space. Recently Cox (2005) wrote a review paper about the three-phase interstellar medium.

Megier *et al.* (2005) pointed out, that the equivalent widths of the Ca II interstellar absorption lines are very well correlated with the distance to the stars. They

proposed to use the Ca II H & K lines to measure the distances to the OB stars. They observed that the equivalent widths of the K I and CH lines are less tightly related to the parallaxes (distances) of stars. They stated that the K I and CH that are present in cloud cores. This observation is in conformance with the McKee & Ostriker model because the cold cloud cores have much lower filling factor than the cloud corona.

An analysis of the interstellar Ti II, Ca II and Na I absorption lines was done by Welsh *et al.* (1997) and by Hunter *et al.* (2006). Column densities of the ionised Ti and Ca are well correlated, yielding a conclusion, that both elements reside in the same environment. Both Ti II and Ca II interstellar lines analysed by them are correlated with distance.

We want to extend the results presented by Megier *et al.* (2005) and include to the analysis elements observed in the ultraviolet spectral range. Because of the difficulties with saturated lines we have used column densities instead of equivalent widths. The Hubble Space Telescope (HST) spectra were used to calculate column densities of Fe II, Ge II, Mg I, Mg II, S I, S II, Si II, Zn II elements. Both GHRS (Goddard High Resolution Spectrograph) and STIS (Space Telescope Imaging Spectrograph) spectra were used.

In the next paragraph we present the method used to determine the column densities. The correlation between column densities and distances is analysed in §3. The relationships between interstellar gas-phase abundances and interstellar reddening E(B-V) or f(H₂) are also presented in §3. The conclusions are summarised in §4.

2 Column Densities

The spectra from the ultraviolet spectral range were downloaded from the HST Data Archive. The GHRS spectra taken in the FP-SPLIT mode were processed with IRAF tasks *poffsets* and *specalign* to achieve the final spectrum. When many spectra for one star were available the column density was calculated independently for each spectrum, and an average column density was determined. The column densities were derived using the profile fitting technique. The absorption lines were fitted by Voigt profiles. The transitions for which the natural damping constant (Γ) is not known (Mg II 1240 Å doublet, Ge II 1237 Å, Mg I 1829 Å) were fitted with a Gauss function. The cloud velocities (v), Doppler broadening parameters (b) and column densities (N) for multiple absorption components were simultaneously fitted to the observed spectrum. Both lines of magnesium doublet (at 2800 Å or 1200 Å) were also fitted simultaneously - v, b and N were common for both lines in the doublet. The wavelengths, oscillator strengths (f) and natural

damping constants (Γ) were adopted from Morton (2003).

A convolution with a point spread function (PSF) was also performed. The PSF for the GHRS consists of two Gaussian components. The "core" Gaussian has a FWHM=1.05 diodes, while the "halo" component has FWHM=5.0 diodes (Spitzer & Fitzpatrick, 1993). The relative contribution of the "core" and "halo" components into the PSF is wavelength dependent and was interpolated from the table given by Cardelli *et al.* (1990). The Gaussian PSF for the STIS spectrograph depends on wavelength, slit and the mode of observations. The tables with FWHM for the combination of mode and slit can be found in "STIS Instrument Handbook" (Kim Quijano *et al.*, 2003). The FWHM of the Gaussian PSF was wavelength-interpolated from these tables. The derived column densities are presented in Table 1.

The interstellar absorption lines of Fe II, Zn II and S II are often saturated. Therefore the column density of these elements was measured only in a few directions. The results for these three elements are fragmentary, because in the directions where the absorption lines were saturated, the column densities were not determined.

3 Results

The column densities of Fe II, Ge II, Mg I, Mg II, S I, S II, Si II, Zn II versus parallaxes are plotted on Fig. 1. The parallaxes of stars used in this paper are taken from the Hipparcos Catalogue (1997).

In order to check how the column density (N) changes with distance (d) a hyperbola was fitted (see Megier *et al.* (2005))

$$\pi = \frac{1}{d} = \frac{1}{a \cdot N + b}$$

in the column density - parallax (π) plane. We do not use the distance, like Hunter *et al.* (2006) or Welsh *et al.* (1997), because only for the parallaxes the plus and minus errors are equal. Moreover, the parallaxes are sometimes negative. Removing such points from the sample leads to the underestimation of distance. The weight for each point in the fitting procedure was equal to $1/\sigma_\pi^2$.

The stars from the Scorpius-Ophiuchus region: HD 141637, HD 143018, HD 144217, HD 147165, HD 147933, HD 148479 belonging to the Upper Scorpius Association (de Zeeuw *et al.*, 1999), and HD 143275, HD 149757 were eliminated from the N- π relation fitting. These are nearby stars lying behind a dense molecular cloud. Therefore these directions have very high column densities and deviate from the N- π relation for other stars. The eliminated stars are shown with open circles on

Fig. 1. The seven stars from the local interstellar medium (LISM) with $\pi > 20$ mas were also excluded from the fitting. The results of the column density - parallax fitting are following:

$$\begin{aligned} d &= (1.23 \pm 0.16) \cdot 10^{-13} \cdot N(MgII) + (89 \pm 8) \quad [pc] \\ d &= (1.72 \pm 0.25) \cdot 10^{-13} \cdot N(SII) + (48 \pm 10) \quad [pc] \\ d &= (1.35 \pm 0.22) \cdot 10^{-13} \cdot N(SiII) + (97 \pm 11) \quad [pc] \\ d &= (3.1 \pm 1.2) \cdot 10^{-11} \cdot N(ZnII) + (96 \pm 38) \quad [pc] \end{aligned}$$

where column densities (N) are in cm^{-2} , and distances are in parsecs. There are no nearby stars with low column density for neutral elements (Mg I, S I) as well as for Ge II. Therefore the hyperbola fit gives very high b term, that should be equal to the Local Bubble dimension. These fits are shown on Fig. 1, but these fits are probably meaningless.

Megier *et al.* (2005) have proposed to use an analogous formula for Ca II to determine the distances to OB stars. In our sample of OB stars objects behind molecular clouds strongly deviate from the column density – distance relation. For example the distance to HD 147933 from the Sco-Oph cloud calculated from the Mg II column density is 6 times greater (800 pc vs. 120 pc) than the distance determined from the Hipparcos parallax ! Such outliers have $f(H_2) > 10^{-2}$, but only some stars with large $f(H_2)$ deviate from the N- π relation.

The column density of Mg II, Si II and Ge II (dominant ionisation stages) normalised to the total hydrogen column density (see Table 2) versus interstellar reddening is presented on Fig. 2. The hydrogen-normalised Si II and Mg II column density drops for sites with more interstellar dust (greater interstellar reddening E(B-V)). For Ge II the drop is not so evident. This can be attributed to the lower condensation temperature of germanium ($T_c(Ge) = 825$ K, versus $T_c(Mg) = T_c(Si) = 1340$ K).

The physical conditions in the interstellar clouds can be characterised by the fractional abundance of molecular hydrogen $f(H_2) = 2N(H_2)/(N(HI) + 2N(H_2))$. The H_2 molecule is in equilibrium between formation on dust grains and gas-phase destruction in chemical processes or in photodissociation. Some elements , such as the noble gas krypton, do not exhibit changes with varying $f(H_2)$, because they do not condense onto dust grains (Cardelli, 1994). On the other hand elements that are easily incorporated into dust grains (Mg, Si) show larger depletions in clouds with large $f(H_2)$ (molecular clouds) – see Fig. 3. Only a slight decrease of germanium abundance was noticed by Cardelli (1994) in a limited sample of directions. In our data (Fig. 3) the increase of germanium depletion is seen in dense, molecular clouds. The errors of Ge abundance are large, due to the weakness of the 1337 Å line.

The abundances of elements in the dominant ionisation stage are lower than

the Solar System abundances for Fe II, Ge II, Mg II and Si II (Fig. 4). The Solar System abundances were adopted from Grevesse & Sauval (2000) and are equal to $(Fe/H)_\odot = 3.16 \cdot 10^{-5}$

$$(Ge/H)_\odot = 3.31 \cdot 10^{-9}$$

$$(Mg/H)_\odot = 3.80 \cdot 10^{-5}$$

$$(Si/H)_\odot = 3.59 \cdot 10^{-5}$$

$$(S/H)_\odot = 1.85 \cdot 10^{-5}$$

$$(Zn/H)_\odot = 4.31 \cdot 10^{-8}$$

In the direction to HD 91316 the Zn II abundance is greater than the Solar System abundance. Zinc is known to not deplete into dust grains, although the Zn abundance may be lower than the Solar System abundance ($[Zn/S] = \log(ZnII/S) - \log(Zn/S)_\odot = -0.13$, Fitzpatrick & Spitzer (1996)). The S II abundance is greater than the Solar System abundance for HD 116658 and HD 68273. Sulphur was known to not incorporate into dust grains. Fitzpatrick & Spitzer (1996) and Fitzpatrick (1996) have stated that the sulphur abundance is close to the solar abundance in diffuse clouds. In our data only 2 of 8 directions have the sulphur abundance close to the solar abundance. The depletion of sulphur reaches $[S/H] = -1.59$ for HD 24398. Such low sulphur abundance leads to doubts if sulphur can be used as a tracer of the total hydrogen column density. The low depletion of S and Zn is not surprising, since these elements have much lower condensation temperatures ($T_c(S) = 674$ K, $T_c(Zn) = 684$ K) than other analysed elements (for Fe, Mg and Si $T_c \sim 1340$ K). The sin-like pattern seen on Fig. 4 is caused by changes in the interstellar reddening E(B-V) in the analysed directions.

Star	Par	FeII	GeII	MgI	MgII	Si	SII	SiII	ZnII
BD+28 4211	9.63±1.71	—	—	$9.18 \pm 0.91 \cdot 10^{11}$	$5.28 \pm 1.90 \cdot 10^{13}$	—	$6.93 \pm 0.28 \cdot 10^{14}$	$1.28 \pm 0.05 \cdot 10^{14}$	—
Feige 24	13.44±3.62	—	—	—	—	—	$7.53 \pm 2.64 \cdot 10^{13}$	$2.76 \pm 0.15 \cdot 10^{13}$	—
GD246	—	—	—	—	—	—	—	$9.80 \pm 0.20 \cdot 10^{13}$	—
HD 432	59.89±0.56	$2.04 \pm 0.17 \cdot 10^{12}$	—	—	$3.65 \pm 0.04 \cdot 10^{12}$	—	—	—	—
HD 11443	50.87±0.82	$3.31 \pm 0.77 \cdot 10^{12}$	—	—	$7.52 \pm 0.04 \cdot 10^{12}$	—	—	—	—
HD 18100	0.88±1.04	$3.39 \pm 0.08 \cdot 10^{14}$	—	$1.72 \pm 0.06 \cdot 10^{12}$	—	—	—	—	—
HD 22049	310.75±0.85	—	—	—	$3.66 \pm 0.18 \cdot 10^{12}$	—	—	—	—
HD 22468	34.52±0.87	—	—	—	$2.55 \pm 0.33 \cdot 10^{12}$	—	—	—	—
HD 23630	8.87±0.99	—	—	$1.07 \pm 0.03 \cdot 10^{12}$	$1.06 \pm 0.15 \cdot 10^{15}$	—	$4.30 \pm 1.71 \cdot 10^{14}$	$8.44 \pm 0.11 \cdot 10^{14}$	—
HD 24398	3.32±0.75	—	$1.05 \pm 0.02 \cdot 10^{12}$	—	$2.38 \pm 0.003 \cdot 10^{15}$	—	$7.50 \pm 2.23 \cdot 10^{14}$	—	—
HD 24534	1.21±0.94	—	$1.42 \pm 0.11 \cdot 10^{12}$	$7.49 \pm 0.46 \cdot 10^{13}$	$2.71 \pm 0.20 \cdot 10^{15}$	—	—	$2.01 \pm 0.12 \cdot 10^{15}$	—
HD 24760	6.06±0.82	—	$3.65 \pm 0.28 \cdot 10^{11}$	—	$1.32 \pm 0.11 \cdot 10^{15}$	—	$6.14 \pm 2.27 \cdot 10^{14}$	—	—
HD 24912	1.84±0.70	—	—	$2.76 \pm 0.14 \cdot 10^{13}$	$3.93 \pm 0.96 \cdot 10^{15}$	$1.49 \pm 0.06 \cdot 10^{13}$	—	$3.19 \pm 0.06 \cdot 10^{15}$	—
HD 28497	2.07±0.82	—	—	$4.86 \pm 0.11 \cdot 10^{12}$	$1.11 \pm 0.28 \cdot 10^{15}$	—	—	$1.45 \pm 0.05 \cdot 10^{15}$	—
HD 34029	77.29±0.89	$2.71 \pm 0.15 \cdot 10^{12}$	—	—	$6.77 \pm 0.14 \cdot 10^{12}$	—	—	—	—
HD 35149	3.39±0.87	—	$6.83 \pm 1.16 \cdot 10^{11}$	$4.36 \pm 2.13 \cdot 10^{13}$	$3.31 \pm 0.21 \cdot 10^{15}$	$5.78 \pm 0.68 \cdot 10^{12}$	$1.06 \pm 0.32 \cdot 10^{15}$	$2.02 \pm 0.08 \cdot 10^{15}$	$7.43 \pm 0.09 \cdot 10^{12}$
HD 36486	3.56±0.83	$1.04 \pm 0.02 \cdot 10^{14}$	—	—	$1.45 \pm 0.06 \cdot 10^{15}$	—	—	$1.19 \pm 0.06 \cdot 10^{15}$	—
HD 36861	3.09±0.78	—	$7.41 \pm 0.60 \cdot 10^{11}$	—	$4.33 \pm 0.21 \cdot 10^{15}$	—	$1.94 \pm 0.71 \cdot 10^{15}$	—	—
HD 37128	2.43±0.91	$2.12 \pm 0.16 \cdot 10^{14}$	$2.21 \pm 0.54 \cdot 10^{11}$	$3.46 \pm 1.68 \cdot 10^{13}$	$2.14 \pm 0.08 \cdot 10^{15}$	—	—	$2.09 \pm 0.04 \cdot 10^{15}$	—
HD 38666	2.52±0.55	$1.90 \pm 0.02 \cdot 10^{14}$	—	$2.91 \pm 0.47 \cdot 10^{12}$	$1.26 \pm 0.17 \cdot 10^{15}$	—	—	$1.49 \pm 0.05 \cdot 10^{15}$	—
HD 38771	4.52±0.77	—	$3.21 \pm 0.75 \cdot 10^{11}$	—	$2.20 \pm 0.14 \cdot 10^{15}$	—	$1.28 \pm 0.34 \cdot 10^{15}$	—	—
HD 44743	6.53±0.66	—	—	$3.71 \pm 0.22 \cdot 10^{11}$	—	—	—	$2.40 \pm 0.20 \cdot 10^{14}$	—
HD 47839	3.19±0.73	—	—	$7.36 \pm 0.39 \cdot 10^{12}$	$2.90 \pm 0.35 \cdot 10^{15}$	—	$1.93 \pm 0.50 \cdot 10^{15}$	$2.58 \pm 0.05 \cdot 10^{15}$	$6.59 \pm 0.15 \cdot 10^{12}$
HD 57061	1.02±0.71	—	$7.22 \pm 0.41 \cdot 10^{11}$	$1.53 \pm 0.11 \cdot 10^{13}$	$5.33 \pm 0.29 \cdot 10^{15}$	—	—	$4.73 \pm 0.10 \cdot 10^{15}$	$1.44 \pm 0.06 \cdot 10^{13}$
HD 61421	285.93±0.88	—	—	—	$3.65 \pm 0.33 \cdot 10^{12}$	—	—	—	—
HD 62044	26.68±0.79	—	—	—	$4.78 \pm 0.20 \cdot 10^{12}$	—	—	—	—
HD 62509	96.74±0.87	—	—	—	$5.33 \pm 0.65 \cdot 10^{12}$	—	—	—	—
HD 68273	3.88±0.53	$1.06 \pm 0.01 \cdot 10^{14}$	—	—	$7.81 \pm 1.49 \cdot 10^{14}$	—	$1.44 \pm 0.02 \cdot 10^{15}$	$1.01 \pm 0.06 \cdot 10^{15}$	—
HD 74455	1.93±0.57	—	$5.45 \pm 0.51 \cdot 10^{11}$	$1.08 \pm 0.03 \cdot 10^{13}$	$3.07 \pm 0.01 \cdot 10^{15}$	$2.36 \pm 0.49 \cdot 10^{12}$	$3.08 \pm 0.02 \cdot 10^{15}$	$3.51 \pm 0.06 \cdot 10^{15}$	—
HD 89688	1.86±0.80	—	—	—	—	$2.35 \pm 0.25 \cdot 10^{13}$	—	$3.25 \pm 0.44 \cdot 10^{15}$	—
HD 91316	0.57±0.82	—	$2.78 \pm 0.73 \cdot 10^{11}$	$5.22 \pm 1.50 \cdot 10^{12}$	$2.57 \pm 0.54 \cdot 10^{15}$	—	—	$2.57 \pm 0.10 \cdot 10^{15}$	$7.95 \pm 0.52 \cdot 10^{12}$
HD 100340	0.70±1.45	—	—	—	—	—	$1.94 \pm 0.10 \cdot 10^{15}$	—	—
HD 111812	10.62±0.90	—	—	—	$3.61 \pm 0.03 \cdot 10^{12}$	—	—	—	—
HD 116658	12.44±0.86	—	—	—	$5.51 \pm 1.73 \cdot 10^{13}$	—	$2.07 \pm 0.09 \cdot 10^{14}$	$1.78 \pm 1.39 \cdot 10^{13}$	—
HD 119608	0.77±0.82	—	—	$1.27 \pm 0.24 \cdot 10^{13}$	$7.97 \pm 1.03 \cdot 10^{15}$	—	—	$4.60 \pm 0.27 \cdot 10^{15}$	$1.88 \pm 0.15 \cdot 10^{13}$
HD 122879	-0.05±0.76	—	—	$1.80 \pm 0.26 \cdot 10^{13}$	$1.60 \pm 0.04 \cdot 10^{16}$	—	—	$1.22 \pm 0.05 \cdot 10^{16}$	—
HD 141637	6.25±0.91	—	$2.45 \pm 0.50 \cdot 10^{12}$	$1.08 \pm 0.02 \cdot 10^{13}$	$7.41 \pm 0.19 \cdot 10^{15}$	—	—	$3.21 \pm 0.18 \cdot 10^{15}$	$1.38 \pm 0.03 \cdot 10^{13}$
HD 143018	7.10±0.84	—	$6.39 \pm 0.94 \cdot 10^{11}$	$1.39 \pm 0.06 \cdot 10^{12}$	$2.62 \pm 0.13 \cdot 10^{15}$	—	$2.02 \pm 0.03 \cdot 10^{15}$	$2.26 \pm 0.04 \cdot 10^{15}$	—
HD 143118	6.61±0.78	—	—	—	$4.47 \pm 1.45 \cdot 10^{14}$	—	—	$4.50 \pm 0.60 \cdot 10^{14}$	$1.31 \pm 0.12 \cdot 10^{12}$
HD 143275	8.12±0.88	—	$1.12 \pm 0.06 \cdot 10^{12}$	$1.65 \pm 0.02 \cdot 10^{13}$	$5.71 \pm 0.25 \cdot 10^{15}$	$2.57 \pm 0.14 \cdot 10^{12}$	—	$4.11 \pm 0.47 \cdot 10^{15}$	—
HD 144217	6.15±1.12	—	—	$1.05 \pm 0.65 \cdot 10^{13}$	—	$3.20 \pm 0.47 \cdot 10^{12}$	—	$4.16 \pm 0.09 \cdot 10^{15}$	$1.50 \pm 0.11 \cdot 10^{13}$
HD 147165	4.44±0.81	—	$3.02 \pm 0.03 \cdot 10^{12}$	$1.58 \pm 0.17 \cdot 10^{13}$	$8.89 \pm 0.24 \cdot 10^{15}$	$3.95 \pm 0.46 \cdot 10^{12}$	—	$4.93 \pm 0.29 \cdot 10^{15}$	—
HD 147933	8.27±1.18	—	$2.20 \pm 0.46 \cdot 10^{12}$	$3.12 \pm 0.26 \cdot 10^{13}$	$5.79 \pm 0.64 \cdot 10^{15}$	$3.52 \pm 0.63 \cdot 10^{13}$	—	$3.60 \pm 0.20 \cdot 10^{15}$	—
HD 148479	5.40±1.68	—	$1.92 \pm 0.26 \cdot 10^{12}$	$4.32 \pm 0.63 \cdot 10^{12}$	$1.67 \pm 0.08 \cdot 10^{16}$	$2.89 \pm 1.46 \cdot 10^{12}$	—	$6.37 \pm 0.06 \cdot 10^{15}$	—
HD 149499	26.94±1.88	—	—	—	—	—	$1.13 \pm 0.17 \cdot 10^{14}$	$7.39 \pm 0.44 \cdot 10^{12}$	—

Star	Par	FeII	GeII	MgI	MgII	Si	SII	SiII	ZnII
HD 149757	7.12±0.71	—	$8.98 \pm 2.38 \cdot 10^{11}$	$2.38 \pm 2.11 \cdot 10^{13}$	$2.61 \pm 0.22 \cdot 10^{15}$	$3.42 \pm 0.46 \cdot 10^{13}$	—	$2.10 \pm 0.04 \cdot 10^{15}$	—
HD 154368	2.73±0.96	—	$3.68 \pm 1.58 \cdot 10^{12}$	—	$1.04 \pm 0.11 \cdot 10^{16}$	$3.41 \pm 0.92 \cdot 10^{13}$	—	$5.81 \pm 0.61 \cdot 10^{15}$	—
HD 158926	4.64±0.90	—	—	$1.05 \pm 0.29 \cdot 10^{11}$	—	—	—	$1.56 \pm 0.41 \cdot 10^{14}$	—
HD 160578	7.03±0.73	—	—	$8.96 \pm 2.33 \cdot 10^{11}$	$4.39 \pm 0.57 \cdot 10^{14}$	—	—	$9.19 \pm 0.16 \cdot 10^{14}$	$4.21 \pm 0.26 \cdot 10^{12}$
HD 195965	1.91±0.58	—	$1.39 \pm 0.28 \cdot 10^{12}$	$4.67 \pm 0.84 \cdot 10^{13}$	$7.96 \pm 0.80 \cdot 10^{15}$	$1.73 \pm 0.17 \cdot 10^{13}$	—	$5.56 \pm 0.14 \cdot 10^{15}$	—
HD 198478	1.45±0.55	—	$3.19 \pm 0.25 \cdot 10^{12}$	—	$8.17 \pm 0.80 \cdot 10^{15}$	—	—	—	—
HD 201345	0.61±0.77	—	—	—	$9.14 \pm 0.80 \cdot 10^{15}$	—	—	—	—
HD 202904	3.62±0.56	—	—	$2.90 \pm 0.33 \cdot 10^{12}$	$1.58 \pm 0.24 \cdot 10^{15}$	—	—	$1.21 \pm 0.04 \cdot 10^{15}$	$6.09 \pm 0.15 \cdot 10^{12}$
HD 203374	-0.70±0.70	—	$2.76 \pm 0.31 \cdot 10^{12}$	$1.11 \pm 0.06 \cdot 10^{14}$	$1.22 \pm 0.05 \cdot 10^{16}$	$4.45 \pm 0.11 \cdot 10^{13}$	—	$1.41 \pm 0.19 \cdot 10^{16}$	—
HD 203664	2.23±1.08	—	—	$1.26 \pm 0.67 \cdot 10^{13}$	$2.93 \pm 0.59 \cdot 10^{15}$	—	—	$4.37 \pm 0.23 \cdot 10^{15}$	—
HD 206267	2.78±0.79	—	$2.92 \pm 0.21 \cdot 10^{12}$	$1.80 \pm 0.09 \cdot 10^{14}$	$1.05 \pm 0.05 \cdot 10^{16}$	—	—	$1.26 \pm 0.15 \cdot 10^{16}$	—
HD 207198	1.62±0.48	—	—	—	$1.15 \pm 0.05 \cdot 10^{16}$	—	—	—	—
HD 207538	0.30±0.62	—	—	—	$1.06 \pm 0.06 \cdot 10^{16}$	—	—	—	—
HD 209339	0.14±0.57	—	$2.31 \pm 0.17 \cdot 10^{12}$	$1.02 \pm 0.11 \cdot 10^{14}$	$1.06 \pm 0.02 \cdot 10^{16}$	$2.56 \pm 0.13 \cdot 10^{13}$	—	$9.43 \pm 1.43 \cdot 10^{15}$	—
HD 210839	1.98±0.46	—	$3.12 \pm 0.92 \cdot 10^{12}$	$1.43 \pm 0.06 \cdot 10^{14}$	$1.13 \pm 0.06 \cdot 10^{16}$	$4.34 \pm 0.15 \cdot 10^{13}$	—	$1.05 \pm 0.07 \cdot 10^{16}$	—
HD 212571	2.96±0.71	—	—	$1.29 \pm 0.77 \cdot 10^{13}$	$2.50 \pm 0.30 \cdot 10^{15}$	$2.88 \pm 0.69 \cdot 10^{12}$	—	$2.23 \pm 0.04 \cdot 10^{15}$	—
HD 219188	0.94±1.16	—	—	$1.36 \pm 0.18 \cdot 10^{13}$	$3.95 \pm 0.20 \cdot 10^{15}$	—	—	$3.54 \pm 0.18 \cdot 10^{15}$	—
HZ 43	31.26±8.33	—	—	—	$1.84 \pm 0.26 \cdot 10^{12}$	—	—	—	—

Table 1: Parallaxes [mas] and column densities [cm^{-2}] for the analysed directions.

4 Conclusions

- The column density of ionised elements Mg II, S II, Si II, Zn II correlates with the distance.
- Estimation of a distance from the column density can lead to large overestimation of the distance for star lying behind molecular clouds.
- Sulphur is depleted in comparison to the Solar System abundance. Sulphur should not be used as a tracer of the hydrogen column density.
- Germanium abundance drops with increasing fractional abundance of molecular hydrogen.

Acknowledgements. The authors would like to thank professor Jacek Krełowski for helpful suggestions. This publication is based on observations made with the NASA/ESA Hubble Space Telescope, obtained from the data archive at the Space Telescope Science Institute. STScI is operated by the Association of Universities for Research in Astronomy, Inc. under NASA contract NAS 5-26555. This work was supported by University of Gdańsk grant BW/5400-5-0219-6.

References

- [Bohlin *et al.* (1978)] Bohlin R.C., Savage B.D., Drake J.F., 1978, ApJ, 224, 132
- [Cardelli *et al.* (1990)] Cardelli, J.A., Ebbets, D.C., Savage, B.D., 1990, ApJ, 365, 789
- [Cardelli (1994)] Cardelli, J., Science, 1994, 265, 209
- [Cox (2005)] Cox, D.P., 2005 , ARAA, 43, 337
- [Diplas & Savage (1994)] Diplas A., Savage B.D., 1994, ApJS, 93, 211
- [Fitzpatrick (1996)] Fitzpatrick, E.L., 1996, ApJ, 473, L55
- [Fitzpatrick & Spitzer (1996)] Fitzpatrick, E.L., Spitzer, L., 1996, ApJ, 475, 623
- [Grevesse & Sauval (2000)] Grevesse, N., Sauval, A.J., 2000, Urania, 690, 248
- [Hipparcos (1997)] "The Hipparcos and Tycho Catalogue", ESA, 1997, SP-1200
- [Hunter *et al.* (2006)] Hunter, I., Smoker, J.V., Keenan, F.P., Ledoux, C., Jehin, E., Cabanac, R., Melo, C., Bagnulo, S., 2006 , MNRAS, 369, 1143

HD	SpType	E(B-V)	N(HI)	err N(HI)	ref.	N(H ₂)	err N(H ₂)	ref.	H _{total}	err H _{total}	f(H ₂)
BD +28 4211	Op	-	-	-	-	-	-	-	-	-	-
Feige 24	DAw	-	-	-	-	-	-	-	-	-	-
GD 246	DAw	-	-	-	-	-	-	-	-	-	-
HD 432	F2IV	-	-	-	-	-	-	-	-	-	-
HD 11443	F6IV	-	-	-	-	-	-	-	-	-	-
HD 18100	B5II/III	-0.045	1.38E+20	3.80E+19	2	-	-	-	-	-	-
HD 22049	K2V	-0.030	-	-	-	-	-	-	-	-	-
HD 22468	G9V	0.112	-	-	-	-	-	-	-	-	-
HD 23630	B7III	0.063	-	-	-	3.46E+19	1.18E+19	3	-	-	-
HD 24398	B1Iab:	0.273	6.40E+20	6.00E+19	4	4.70E+20	2.00E+20	4	1.58E+21	4.60E+20	5.95E-01
HD 24534	O9.5pe	0.290	5.37E+20	6.93E+19	5	8.32E+20	7.32E+19	5	2.20E+21	2.16E+20	7.56E-01
HD 24760	B0.5V+	0.112	2.50E+20	5.00E+19	4	3.30E+19	2.10E+19	4	3.16E+20	9.20E+19	2.09E-01
HD 24912	O7.5IIIe	0.291	1.30E+21	3.00E+20	4	3.40E+20	1.20E+20	4	1.98E+21	5.40E+20	3.43E-01
HD 28497	B2V:ne	0.042	1.60E+20	3.20E+19	1	6.60E+14	-	1	1.60E+20	3.20E+19	8.25E-06
HD 34029	G5IIIe+	-0.060	-	-	-	-	-	-	-	-	-
HD 35149	B1V	0.110	5.50E+20	1.10E+20	1	<3.40E+18	-	1	5.50E+20	1.10E+20	-
HD 36486	O9.5II+	0.080	1.70E+20	3.40E+19	1	4.80E+14	-	1	1.70E+20	3.40E+19	5.65E-06
HD 36861	O8III	0.490	6.00E+20	1.50E+20	1	1.32E+19	-	1	6.26E+20	1.50E+20	4.21E-02
HD 37128	B0Iab:	0.040	2.80E+20	5.60E+19	1	3.70E+16	-	1	2.80E+20	5.60E+19	2.64E-04
HD 38666	O9.5V	0.046	7.00E+19	1.40E+19	1	3.20E+15	-	1	7.00E+19	1.40E+19	9.14E-05
HD 38771	B0Iab:	0.118	3.30E+20	3.30E+19	1	4.80E+15	-	1	3.30E+20	3.30E+19	2.91E-05
HD 44743	B1II/III	0.030	<5.00E+18	-	1	<2.00E+17	-	1	-	-	-
HD 47839	O7Ve	0.070	2.50E+20	5.00E+19	1	3.50E+15	-	1	2.50E+20	5.00E+19	2.80E-05
HD 57061	O9lb	0.130	5.00E+20	5.00E+19	1	3.00E+15	-	1	5.00E+20	5.00E+19	1.20E-05
HD 61421	F5IV-V	-0.031	-	-	-	-	-	-	-	-	-
HD 62044	K1III	0.050	-	-	-	-	-	-	-	-	-
HD 62509	K0IIIb	0.000	-	-	-	-	-	-	-	-	-
HD 68273	WCvar+	-	6.00E+19	6.00E+18	1	1.70E+14	-	1	6.00E+19	6.00E+18	5.67E-06
HD 74455	B1.5Vn	0.081	5.37E+20	7.99E+19	2	-	-	-	-	-	-
HD 89688	B3.2IV	0.107	-	-	-	-	-	-	-	-	-
HD 91316	B1Iab	0.042	1.80E+20	3.60E+19	1	4.10E+15	-	1	1.80E+20	3.60E+19	4.56E-05
HD 100340	B9	-	2.95E+20	3.81E+19	2	-	-	-	-	-	-
HD 111812	G0IIIp	-0.023	-	-	-	-	-	-	-	-	-
HD 116658	B1III-IV+	0.130	1.00E+19	2.50E+18	1	8.90E+12	-	1	1.00E+19	2.50E+18	1.78E-06
HD 119608	B1lb	0.120	7.76E+20	2.14E+20	2	-	-	-	-	-	-
HD 122879	B0Ia	0.298	-	-	-	-	-	-	-	-	-
HD 141637	B1.5Vn	0.178	1.55E+21	3.10E+20	1	1.70E+19	-	1	1.58E+21	3.10E+20	2.15E-02
HD 143018	B1V+	0.070	5.20E+20	5.20E+19	1	2.10E+19	-	1	5.62E+20	5.20E+19	7.47E-02
HD 143118	B2.5IV	0.019	-	-	-	-	-	-	-	-	-
HD 143275	B0.2IVe	0.209	1.40E+21	2.80E+20	1	2.60E+19	-	1	1.45E+21	2.80E+20	3.58E-02
HD 144217	B0.5V	0.210	1.24E+21	1.24E+20	1	6.70E+19	-	1	1.37E+21	1.24E+20	9.75E-02
HD 147165	B1III	0.357	2.20E+21	8.80E+20	1	6.10E+19	-	1	2.32E+21	8.80E+20	5.25E-02
HD 147933	B2/B3V	0.460	4.27E+21	7.98E+20	2	3.70E+20	-	1	5.01E+21	7.98E+20	1.48E-01
HD 148479	B2V	0.240	-	-	-	-	-	-	-	-	-
HD 149499	K0V	-0.110	-	-	-	-	-	-	-	-	-
HD 149757	O9V	0.327	5.20E+20	2.60E+19	4	4.40E+20	-	4	1.40E+21	2.60E+19	6.29E-01
HD 154368	O9Ia	0.665	1.00E+21	1.09E+20	5	1.45E+21	2.15E+20	5	3.89E+21	5.39E+20	7.43E-01
HD 158926	B2IV+...	0.100	<2.40E+19	-	1	5.00E+12	-	1	-	-	-
HD 160578	B1.5III	0.083	1.55E+20	3.19E+19	2	<1.70E+14	-	3	1.55E+20	3.19E+19	-
HD 195965	B0V	0.225	7.94E+20	1.49E+20	2	-	-	-	-	-	-
HD 198478	B3Iae	0.439	-	-	-	-	-	-	-	-	-
HD 201345	O9p	-0.140	7.41E+20	1.52E+20	2	-	-	-	-	-	-
HD 202904	B2Vne	0.130	4.79E+20	1.40E+20	3	1.41E+19	4.79E+18	3	5.07E+20	1.49E+20	5.57E-02
HD 203374	B0IVpe	0.513	1.29E+21	2.41E+20	2	-	-	-	-	-	-
HD 203664	B0.5III	0.075	3.47E+20	7.76E+19	2	-	-	-	-	-	-
HD 206267	O6e	0.210	2.00E+21	7.00E+20	4	7.20E+20	6.50E+19	4	3.44E+21	8.30E+20	4.19E-01
HD 207198	O9IIe	0.537	2.19E+21	7.09E+20	5	6.76E+20	5.95E+19	1	3.54E+21	8.28E+20	3.82E-01
HD 207538	O9V	0.560	2.20E+21	6.00E+20	4	8.10E+20	7.60E+19	4	3.82E+21	7.52E+20	4.24E-01
HD 209339	B0IV	0.304	-	-	-	-	-	-	-	-	-
HD 210839	O6Iab:	0.481	1.41E+21	2.91E+20	5	6.92E+20	6.09E+19	5	2.80E+21	4.12E+20	4.95E-01
HD 212571	B1Ve	0.092	-	-	-	-	-	-	-	-	-
HD 219188	B0.5III	0.075	7.00E+20	2.80E+20	1	2.20E+19	-	1	7.44E+20	2.80E+20	5.91E-02
HZ 43	DAw	-	-	-	-	-	-	-	-	-	-

Table 2: Interstellar reddening and hydrogen column density for target stars. References: 1 - Bohlin *et al.* (1978) ; 2 - Diplas & Savage (1994) ; 3 - Jenkins *et al.* (1986) ; 4 - Lacour *et al.* (2005) ; 5 - Rachford *et al.* (2002).

- [Jenkins *et al.* (1986)] Jenkins E.B., Savage B.D., Spitzer L., 1986, ApJ, 301, 355
- [Kim Quijano (2003)] Kim Quijano, J. *et al.*, 2003, "STIS Instrument Handbook" (Baltimore: STScI), available at: <http://www.stsci.edu/hst/stis/documents>
- [Lacour *et al.* (2005)] Lacour S., André, M.K., Sonnentrucker, P., *et al.* , 2005, A&A, 430, 967
- [McKee & Ostriker (1977)] McKee, Ch.F., Ostriker, J.P., 1977 , ApJ, 218, 148
- [Megier *et al.* (2005)] Megier, A., Strobel, A., Bondar, A., Musaev, F.A, Inwoo Han, Krełowski, J., Galazutdinov, G.A., 2005 , ApJ, 634, 451
- [Morton (2003)] Morton, D.C., 2003, ApJSS, 149, 205
- [Rachford *et al.* (2002)] Rachford B.L., et al., 2002, ApJ, 577, 221
- [Spitzer & Fitzpatrick (1993)] Spitzer, L.Jr., Fitzpatrick, E.L., 1993, ApJ, 409, 299
- [Welsh *et al.* (1997)] Welsh, B.Y., Sasseen, T., Craig, N., Jelinsky, S., Albert, C.E., 1997, ApJSS, 112, 507
- [de Zeeuw *et al.* (1999)] de Zeeuw, P.T., Hoogerwerf, R., de Bruijne, J.H.J., Brown, A.G.A, Blaauw, A., 1999 , AJ, 117, 354

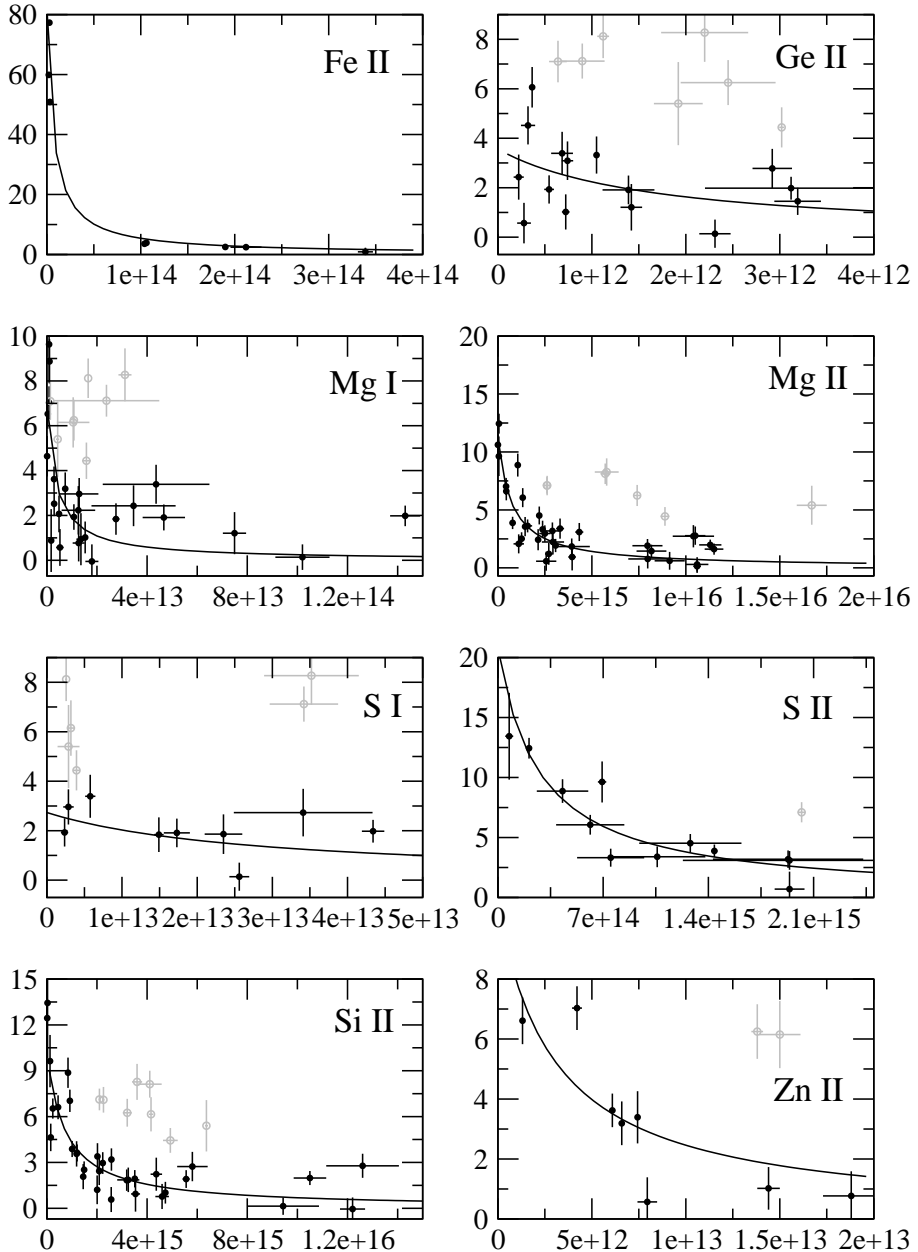


Figure 1: Column densities [cm⁻²] versus parallaxes [mas]. The grey open circles represents stars from the Scorpius – Ophiuchus region.

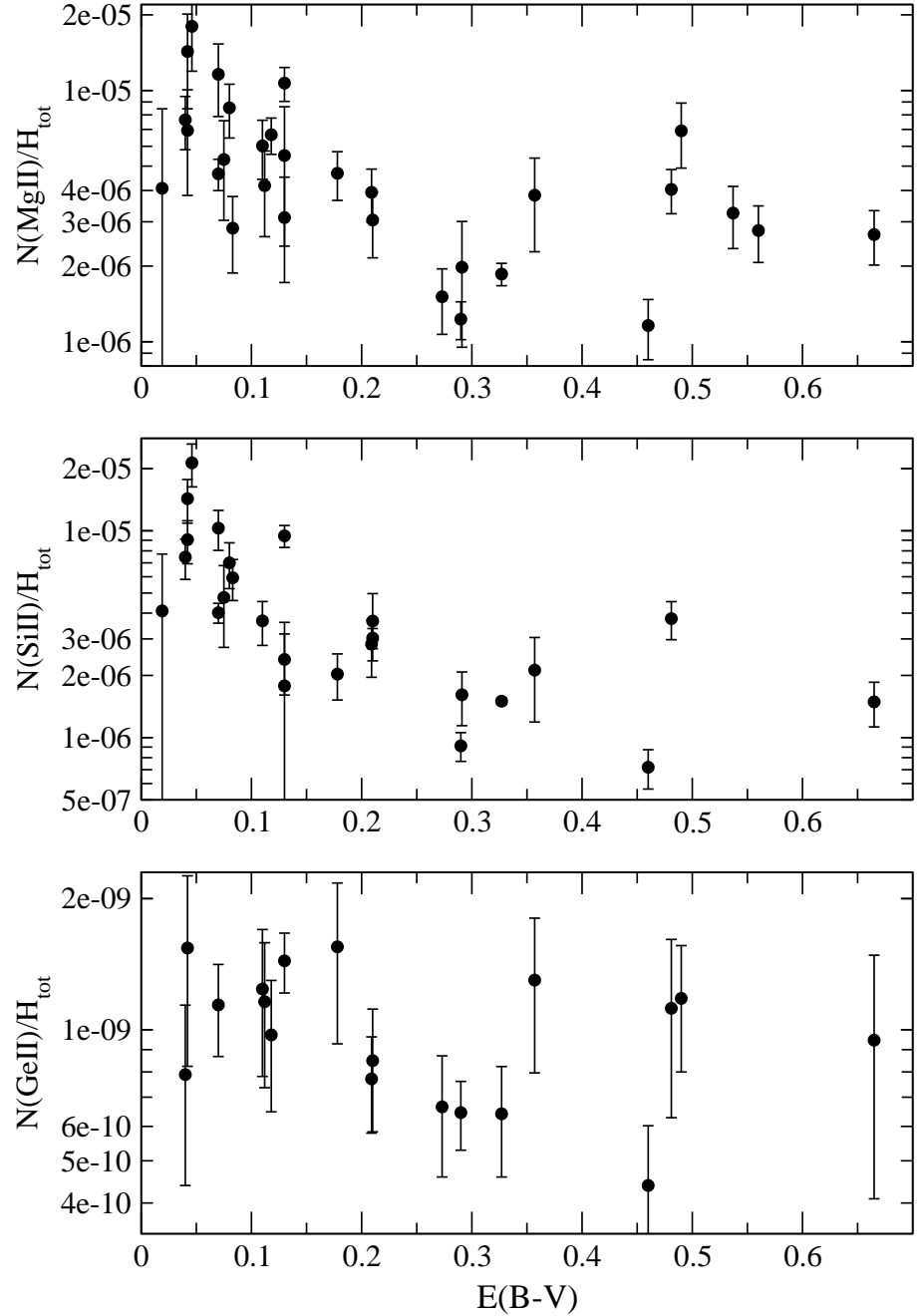


Figure 2: Column densities of Mg II, Si II and Ge II normalised to the total hydrogen column density (logarithmic scale) versus the interstellar reddening $E(B-V)$.

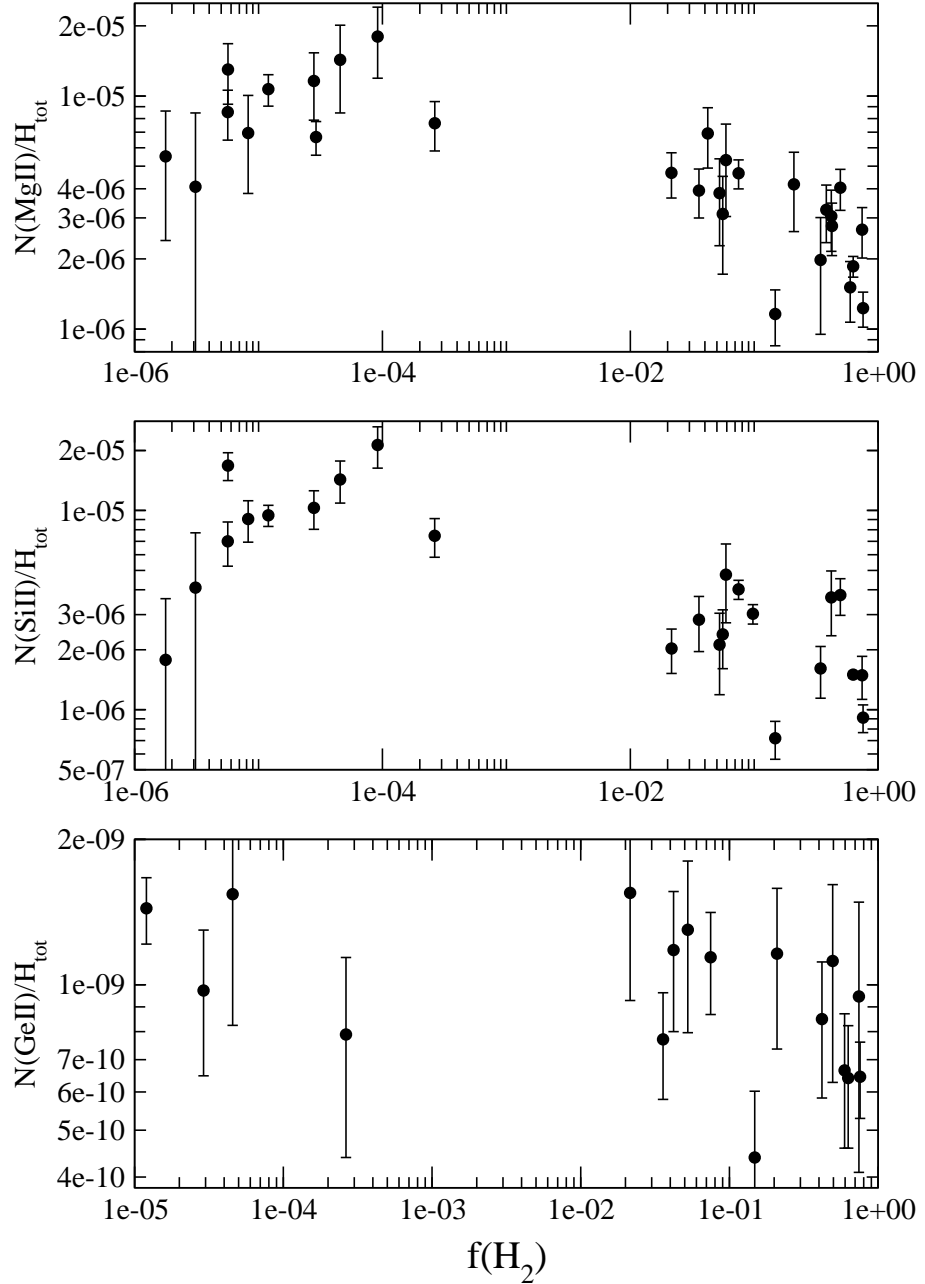


Figure 3: Column densities of Mg II, Si II and Ge II normalised to the total hydrogen column density versus fractional abundance of molecular hydrogen $f(\text{H}_2)$. Both axis use logarithmic scale.

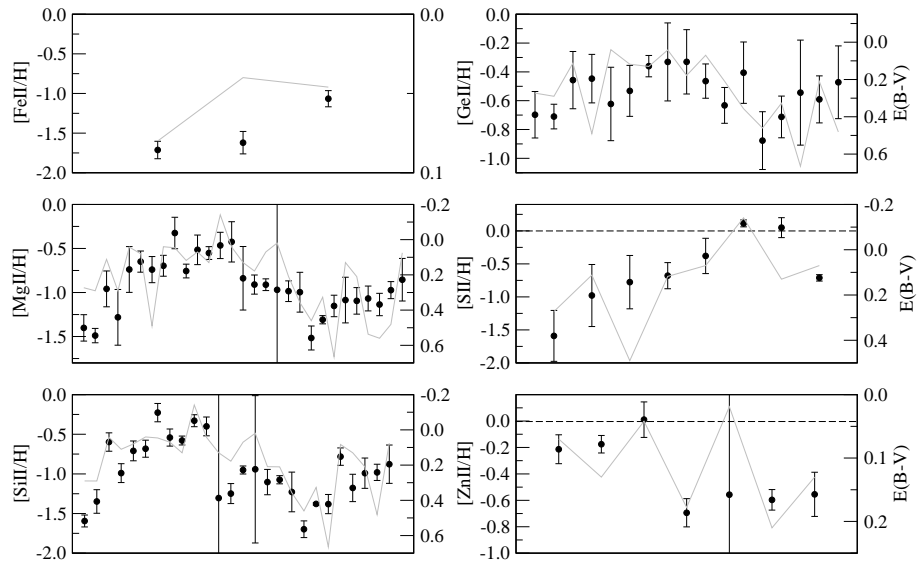


Figure 4: Black dots show the abundance of the dominant ionization stage relative to the Solar System abundance [dex]. The grey lines represent the interstellar reddening $E(B-V)$. The stars are ordered by HD numbers.